O.G.Tchikilev IHEP, Protvino

Outline of the talk

- E.K.Sarkisyan, A.S.Sakharov, On similarities of bulk obsevables in nuclear and particle collisions, hep-ph/0410324 , ISMD2005, August 2005, Kromeriz, CZ
- S.J.Lee, A.Z.Mekjan, Nuclear Physics A730(2004)514-547, Development of particle multiplicity distributions using a general form of the grand canonical partition function

hep-ph/0410324
CERN-PH-TH/2004-213

On similarities of bulk observables in nuclear and particle collisions

Edward K.G. Sarkisyan[a,b] and Alexander S. Sakharov[a,c,d]

[a] *Department of Physics, CERN, CH-1211 Geneva 23, Switzerland*
[b] *Department of Physics, the University of Manchester, Manchester M13 9PL, UK*
[c] *Swiss Institute of Technology, ETH-Zürich, 8093 Zürich, Switzerland*
[d] *INFN Laboratory Nazionali del Gran Sasso, SS. 17bis 67010 Assergi (L'Aquila), Italy*

Abstract

We study the regularities in the multiparticle production data obtained from different types of collisions indicating the universality of the hadroproduction process. The similarities of such bulk variables like the charged particle mean multiplicity and the pseudorapidity density at midrapidity measured in nucleus-nucleus, (anti)proton-proton and e^+e^- interactions are analysed according to the dissipating energy of participants and their types. This approach shows a good agreement with the measurements in a wide range of nuclear collision energies from AGS to RHIC. The predictions up to the LHC energies are made and compared to experimental extrapolations.

at midrapidity as a function of c.m. energy, from most central nucleus-nucleus collisions at RHIC [6,10,27,50,51], CERN SPS [52–55], and AGS [56] *vs.* those measured in pp/$\bar{\rm p}$p interactions at CERN [4,30,32,57] and Fermilab [5,34,59]. The comparison is given the same way as the mean multiplicity is shown in Fig. 1, *i.e.* the data from nucleus-nucleus collisions are plotted at the energy $\sqrt{s_{\rm NN}} = \sqrt{s_{\rm pp}}/3$. One can again see that up to the existing $\sqrt{s_{\rm NN}}$, the data from hadronic and nuclear experiments are close to each other being consistent with our interpretation. The measurements from the two types of collisions coincide at 8 GeV $< \sqrt{s_{\rm NN}} <$ 20 GeV and are of the magnitude of the spread of heavy-ion data points at the highest energy of 200 GeV. For a few GeV energy shown, one can also see the visible difference. The data shown in Fig. 2 indicates that the deviation between the two types of collisions increases with the c.m. energy due to faster increase of the midrapidity density values obtained in heavy-ion collisions in comparison with those measured in $\bar{\rm p}$p interactions. At lower energies too, the nuclear data, being lower than the pp data, increases faster. The latter means that, as we discussed above, in contrast to the mean multiplicity, which is in general defined by the total yield of the reaction, so being less sensitive to reaction details, the midrapidity density depends on some additional factor. As the midrapidity density is measured in the very central region, where the participants longitudinal velocities are zeroed, it is natural to assume that this factor is related to the size of the Lorentz-contracted volume of the initial thermalized system determined by participating patterns.

To take into account the corresponding correction, let us consider our picture in the framework of the Landau model which reasonably well describes the bulk variables measured and is, by its nature, near to our interpretation as discussed above. Using this model, one finds for the ratio of the charged particle rapidity density $\rho(y) = (2/N_{\rm part}) dN_{\rm ch}/dy$ per participant pair at the midrapidity value $y = 0$ in heavy-ion reaction, $\rho_{\rm NN}$, to the density $\rho_{\rm pp}$ in pp/$\bar{\rm p}$p interaction,

$$\frac{\rho_{\rm NN}(0)}{\rho_{\rm pp}(0)} = \frac{2\,N_{\rm ch}}{N_{\rm part}\,N_{\rm ch}^{\rm pp}}\sqrt{\frac{L_{\rm pp}}{L_{\rm NN}}}\,. \tag{1}$$

Here, $N_{\rm part}$ is the number of participants in heavy-ion collision, $N_{\rm ch}$ ($N_{\rm ch}^{\rm pp}$) is the multiplicity in nucleus-nucleus (pp/$\bar{\rm p}$p) collision and $L = \ln\frac{\sqrt{s}}{2m}$, where m is the mass of a participating pattern, *e.g.* of a proton, $m_{\rm p}$, in central heavy-ion collisions. According to our interpretation, we compare in the ratio (1) the rapidity density $\rho_{\rm NN}(0)$ at $\sqrt{s_{\rm NN}}$ to the rapidity density $\rho_{\rm pp}(0)$ at $\sqrt{s_{\rm pp}}/3$. Due to the above, we consider a constituent quark of mass $\frac{1}{3}m_{\rm p}$ as a participating pattern in pp/$\bar{\rm p}$p collisions, and a proton as an effectively structureless participant in most central nucleus-nucleus collisions. Then, from Eq. (1) one obtains:

$$\rho_{\rm NN}(0) = \rho_{\rm pp}(0)\,\frac{2\,N_{\rm ch}}{N_{\rm part}\,N_{\rm ch}^{\rm pp}}\sqrt{1 - \frac{4\ln 3}{\ln\left(4m_{\rm p}^2/s_{\rm NN}\right)}}\,. \tag{2}$$

Using the fact that the transformation factor from rapidity to pseudorapidity does not influence the above ratio and substituting the data values of $N_{\rm ch}$ and $N_{\rm ch}^{\rm pp}$ shown in Fig. 1 and of $\rho_{\rm pp}(0)$ shown in Fig. 2, one obtains from Eq. (2) the values of pseudorapidity density in nucleus-nucleus collisions. These values are displayed in Fig. 2 by solid line. One can see that the correction made provides a good agreement between the calculated $\rho_{\rm NN}(0)$ values and

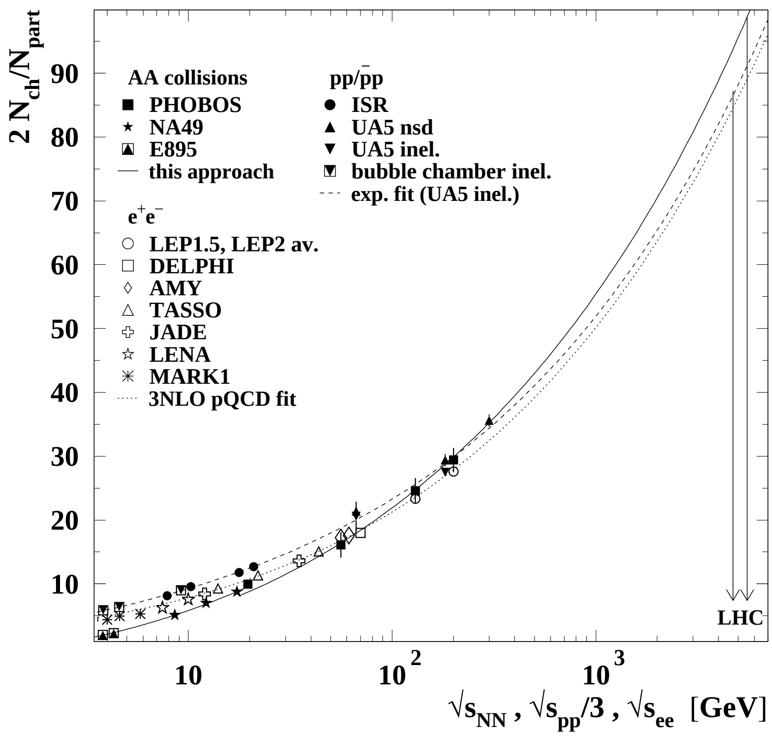

Figure 1: The charged particle mean multiplicity per participant pair as a function of the c.m. energy. The solid and combined symbols show the multiplicity value of the most central heavy-ion (AA) collisions at RHIC as measured by PHOBOS Collaboration (■) in [2,3,26,27], and by NA49 Collaboration at CERN SPS [28] (★) and by E895 Collaboration at AGS [29] (◮) (see also [2]), and, in p̄p collisions, the measurements made at CERN by UA5 Collaboration (▲ for non-single diffractive, ▼ for inelastic events) at $\sqrt{s_{\rm pp}}$ = 546 GeV [30] and $\sqrt{s_{\rm pp}}$ = 200 and 900 GeV [31] and, at lower c.m. energies, in pp collisions obtained at CERN-ISR (•) [32] and from bubble chamber experiments [33,34] (⧩) , the latter compiled and analysed in [35]. (The inelastic UA5 data at $\sqrt{s_{\rm pp}}$ = 200 GeV is extrapolated in [15] from the limited rapidity range to the full one.) The open symbols show the e^+e^- measurements: the high-energy LEP mean multiplicities averaged here from the recent data values (○) at LEP1.5 $\sqrt{s_{\rm ee}}$ = 130 GeV in [36,37] and LEP2 $\sqrt{s_{\rm ee}}$ = 200 GeV in [37,38], and the lower-energy data as measured by DELPHI [39] (□), TASSO [40] (△), AMY [41] (◇), JADE [42] (+), LENA [43] (⋆), and MARK1 [44] (⊛) Collaborations. (See also [45–47] for data on e^+e^- and pp/p̄p collisions). The solid line shows the calculations from Eq. (2) based on our approach and using the corresponding fits (see text). The dashed and dotted lines show the fit to the pp/p̄p data from [30] and the 3NLO perturbative QCD fit [48] to e^+e^- data by ALEPH [37]. The arrows show the expectations for the LHC.

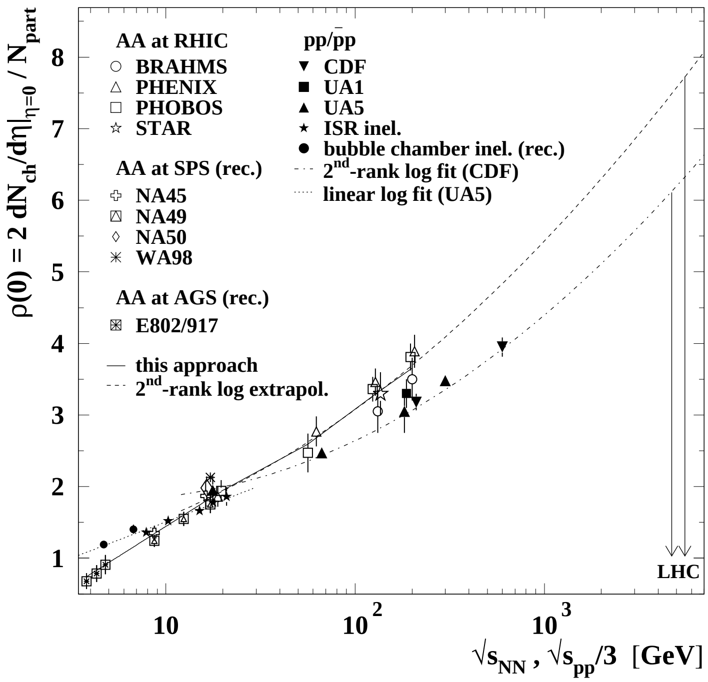

Figure 2: Pseudorapidity density of charged particles per participant pair at midrapidity as a function of the c.m. energy of collision. The open and combined symbols show the pseudorapidity density values per participant pair *vs.* c.m. energy per nucleon, $\sqrt{s_{\rm NN}}$, measured in the most central heavy-ion collisions at RHIC by BRAHMS [50] (○), PHENIX [10] (△), PHOBOS [6,27] (□), and STAR [51] (⋆) Collaborations, and the density values recalculated in [10] from the measurements taken at CERN SPS by CERES/NA45 [52] (+), NA49 [53] (⍂), NA50 [54] (◊) and WA98 [55] (✳) Collaborations and at Fermilab AGS by E802 and E917 Collaborations [56] (⊞). The nuclear data at $\sqrt{s_{\rm NN}}$ around 20 GeV and the RHIC data at $\sqrt{s_{\rm NN}}$ = 130 GeV and 200 GeV are given spread horizontally for clarity. The PHENIX data at $\sqrt{s_{\rm NN}}$ = 62.4 GeV is taken from [11]. The solid symbols show the pseudorapidity density values *vs.* c.m. energy $\sqrt{s_{\rm pp}}/3$ as measured in non-single diffractive p̄p collisions by UA1 [57] (■) and UA5 [4,30] (▲) Collaborations at CERN SPS, by UA5 at CERN ISR ($\sqrt{s_{\rm pp}}$ = 53 GeV), by CDF Collaboration at Fermilab [5] (▼), and in inelastic pp collisions from the ISR [32] (★) and bubble chamber [34,59] (●) experiments. The data from the bubble chamber experiments [34,59] are given as recalculated in [4]. The solid line connects the predictions from Eq. (2). The dashed line gives the fit to the calculations using the 2nd order log-polynomial fit function analogous to that used [5] in p̄p data. The fit function from [5] is shown by the dashed-dotted line. The dotted line shows the linear log approximation of UA5 to inelastic events [4]. The arrows show the expectations for the LHC. Note that e^+e^- data at $\sqrt{s_{\rm ee}}$ = 14 GeV to 200 GeV (not shown) follows the heavy-ion data [3].

Available online at www.sciencedirect.com
SCIENCE DIRECT®
ELSEVIER
Nuclear Physics A 730 (2004) 514–547
NUCLEAR PHYSICS A
www.elsevier.com/locate/npe

Development of particle multiplicity distributions using a general form of the grand canonical partition function

S.J. Lee [a,*], A.Z. Mekjian [b]

[a] *Department of Physics and Institute of Natural Sciences, Kyung Hee University, Suwon, KyungGiDo, South Korea*
[b] *Department of Physics, Rutgers University, Piscataway, NJ, USA*

Received 28 March 2003; received in revised form 15 October 2003; accepted 5 November 2003

Abstract

Various phenomenological models of particle multiplicity distributions are discussed using a general form of a unified model which is based on the grand canonical partition function and Feynman's path integral approach to statistical processes. These models can be written as special cases of a more general distribution which has three control parameters which are a, x, z. The relation to these parameters to various physical quantities are discussed. A connection of the parameter a with Fisher's critical exponent τ is developed. Using this grand canonical approach, moments, cumulants and combinants are discussed and a physical interpretation of the combinants are given and their behavior connected to the critical exponent τ. Various physical phenomena such as hierarchical structure, void scaling relations, Koba–Nielson–Olesen or KNO scaling features, clan variables, and branching laws are shown in terms of this general approach. Several of these features which were previously developed in terms of the negative binomial distribution are found to be more general. Both hierarchical structure and void scaling relations depend on the Fisher exponent τ. Applications of our approach to the charged particle multiplicity distribution in jets of L3 and H1 data are given.

PACS: 25.75.Dw; 25.75.Gz; 24.10.Pa; 05.30.Jp; 05.40.+j

* Corresponding author.
E-mail address: sjlee@physics.rutgers.edu (S.J. Lee).

0375-9474/$ – see front matter
doi:10.1016/j.nuclphysa.2003.11.008

Table 1
Various models with specific choice of $\alpha_k = k$ and x_k in hypergeometric series $F(a,b;c;z)$ of Eq. (44). Here $k=0$ is not included, and thus $f_0 = \ln Z = \sum_{k=1}^{\infty} x_k = xzF(a,b;c;z)$. Here $1 \leqslant k \leqslant N$ with $N \to \infty$ except for Poisson which has a finite Nx. Fisher exponent τ for each x_k as discussed in Section 2.3 are given too

Model	x_k	$f_0(\vec{x}) = \ln Z$	a	b	c	τ
Poisson (P)	$Nx\delta_{k,1}$ or x for $k = 1,2,\dots,N$	$Nx = \bar{A}$				
Geometric (Geo)	xz^k	$\frac{xz}{1-z}$	a	1	a	0
Negative binomial (NB)	$\frac{1}{k}xz^k$	$-x\ln(1-z)$	1	1	2	1
Signal/Noise (SN)	$(y + \frac{x}{k})z^k$	$\frac{yz}{1-z} - x\ln(1-z)$				
Lorentz/Catalan (LC)	$\frac{1}{k}2^{-2(k-1)}\binom{2(k-1)}{k-1}xz^k$	$2x[1-(1-z)^{1/2}]$	$\frac{1}{2}$	1	2	3/2
Hypergeometric (HGa)	$\frac{[a]_{k-1}}{k!}xz^k$	$\frac{x}{1-a}[1-(1-z)^{1-a}]$	a	1	2	$2-a$
Random walk–1d (RW1D)	$2^{-2(k-1)}\binom{2(k-1)}{k-1}xz^k$	$xz(1-z)^{-1/2}$	$\frac{1}{2}$	$1(b)$	$1(b)$	1/2
Random walk–2d (RW2D)	$\left[2^{-2(k-1)}\binom{2(k-1)}{k-1}\right]^2 xz^k$	$xzF(\frac{1}{2},\frac{1}{2};1;z)$	$\frac{1}{2}$	$\frac{1}{2}$	1	1
Generalized RW1D (GRW1D)	$\frac{[a]_{k-1}}{(k-1)!}xz^k$	$xz(1-z)^{-a}$	a	b	b	$1-a$
Generalized RW2D (GRW2D)	$\left[\frac{[a]_{k-1}}{(k-1)!}\right]^2 xz^k$	$xzF(a,a;1;z)$	a	a	1	$2(1-a)$

has in its weight a shifted Catalan number divided by $2^{2(k-1)}$, that is $\frac{[1/2]_{k-1}}{k!} = 2^{-2(k-1)}C_k$, beside the xz^k factor which is the weight for Geo model. The Catalan numbers given by $C_{k+1} = \binom{2k}{k}/(k+1)$ are $1, 2, 5, 14, \dots$ for $k = 1, 2, 3, 4, \dots$ and the shifted Catalan numbers given by $C_k = \binom{2(k-1)}{k-1}/k$ are $1, 1, 2, 5, 14, \dots$. The importance of this factor appears in percolation or splitting dynamics [38,39] which uses ancestral or evolutionary variables.

Of all these distributions, the NB has been the most frequently studied. Ref. [40] gives several sources for its origin. These sources include sequential processes, self-similar cascade models and connections with Cantor sets and fractal structure, generalizations of the Planck distribution, solutions to stochastic differential equations. Becattini [41] have shown that the NB distribution arises from decaying resonances. The α model of Ref. [8], which is a self similar random cascade process, leads to a NB like behavior. The stochastic aspects of the NB distribution have been discussed by Hwa [42]. Hegyi [43] has discussed the NB distribution in terms of combinants. The LC model can be connected to a Ginzburg–Landau approach [39] and also has an underlying splitting or branching dynamics and cascade like features with a branching probability p and survival probability $(1-p)$.

As can be seen from the arguments of the hypergeometric function $F(a,b;c;z)$ in Table 1, the hypergeometric model with $b = 1$ and $c = 2$ (HGa) include Geo, NB, SN, LC as a special case of HGa depending on the value of a. Other models listed in Table 1 are based on random walks. The use of random walk results was originally due to Feynman [44] in his description of the phase transition in liquid helium. The random walk aspects arise when considering the closing of cycle of length k. We include them for completeness. Since the random walk in 1-dimension (RW1D) is the same as LC except the missing $1/k$ dependence compared to LC, RW1D can be extended to a generalized RW1D (GRW1D) similar to the generalization of LC to HGa. A random walk model in 2-dimension has an

Table 3
Various cumulants of charged particle multiplicity distribution of jets for L3 data (all events of e^+e^-) [48] and H1 data (pseudorapidity range $1 < \eta^* < 5$ with 80 GeV $< W <$ 115 GeV of e^+p) [49] compared with models having the same mean and fluctuation

Model	a	x	z	$\langle n\rangle$	ξ	κ_3	χ	chi^2
L3 data				20.463±0.003	0.044238±0.00009	0.008158±0.00007		
HGa	0.5 (LC)	18.948	0.64419	20.463	0.044238	0.005871	0.74726	0.00066
	1.0 (NB)	22.605	0.47514	20.464	0.044238	0.003914	0.71208	0.00085
	2.0 (Geo)	31.123	0.31159	20.463	0.044238	0.002936	0.68841	0.00098
	0.31559	18.007	0.74150	20.463	0.044238	0.008158	0.77636	0.00054
GRW1D	0.14006	20.905	0.66088	20.463	0.044239	0.008158	0.78558	0.00051
H1 data				7.7210±0.043	0.069186±0.0053	−0.000764±0.0065	0.73242	
HGa	0.5 (LC)	10.394	0.51653	7.7210	0.069186	0.014360	0.82028	0.00016
	1.0 (NB)	14.454	0.34819	7.7210	0.069186	0.009573	0.80122	0.00012
	2.0 (Geo)	22.814	0.21079	7.7210	0.069186	0.007180	0.78921	0.00010
	3.0	31.244	0.15115	7.7210	0.069186	0.006382	0.78470	0.00010
GRW1D	−0.85160	−4.4150	−0.81168	7.7211	0.069185	−0.000764	0.72375	0.00014

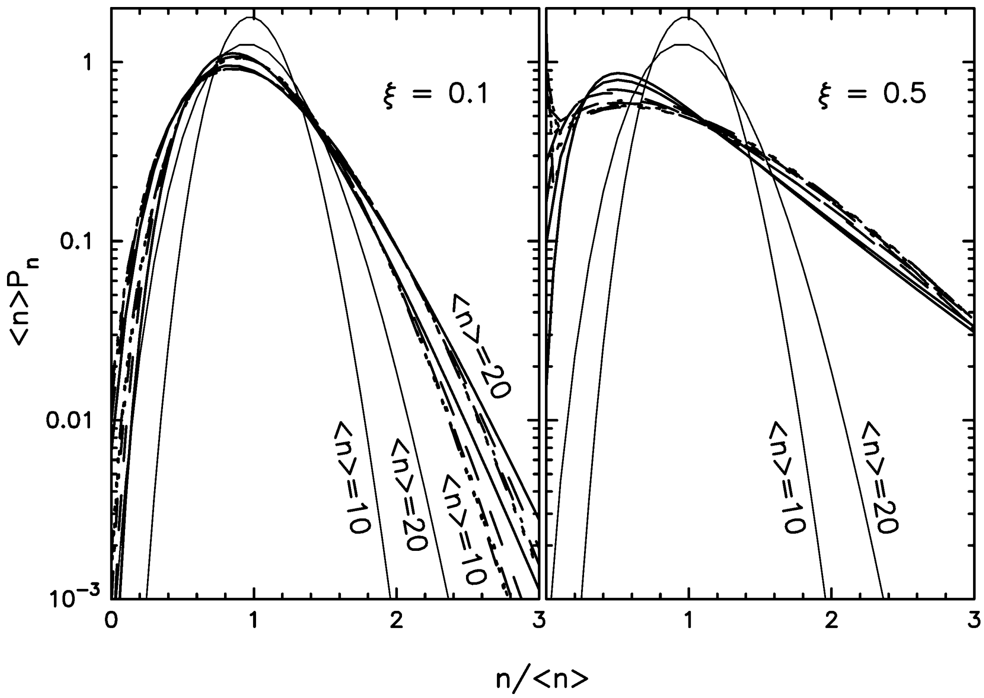

Fig. 4. KNO plot of $\langle n\rangle P_n$ for fixed $\langle n\rangle = 10$ and 20 for $a = 1/2, 1, 2, 3, 4$.

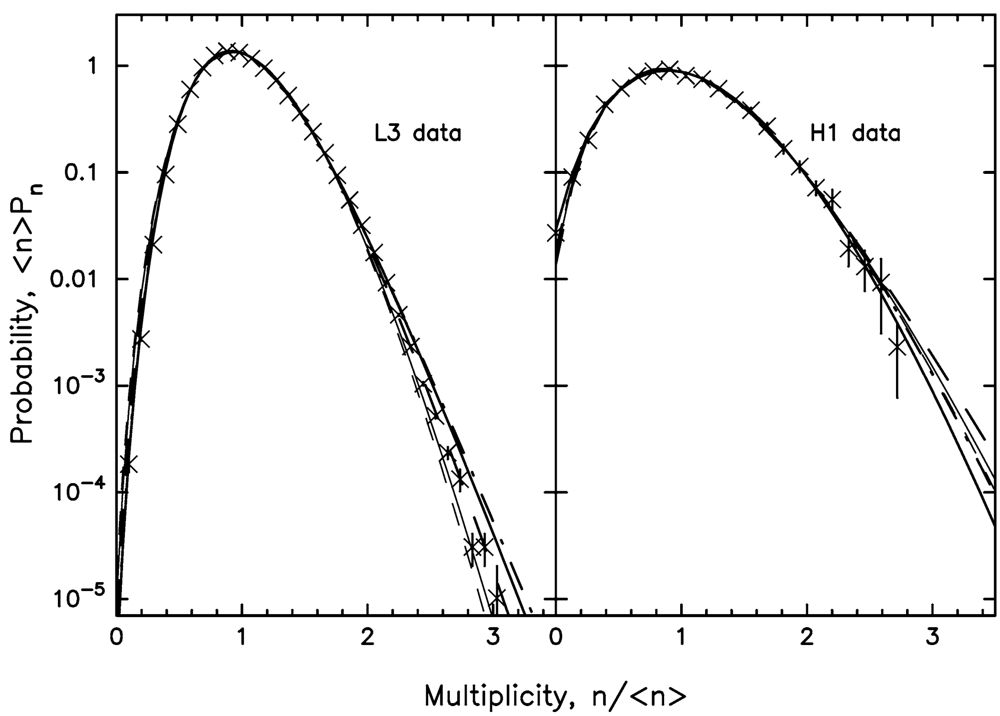

Fig. 5. Charged particle multiplicity distribution in jets of L3 data [48] and H1 data [49]. The crosses are the data and the curves are the fits with HGa and GRW1D given in Table 3. The thick solid curves are the GRW1D fit, the thick dashed curves are LC model, the thin solid curves for NB model, the thin dashed curves for Geo model. The dash-dotted curves are for HGa model with $a = 0.31559$ for L3 data and with $a = 3.0$ for H1 data.

4. Conclusion

Event-by-event studies from high energy collisions are being used to study the details of particle multiplicity distributions as, for example, those associated with pions. Such studies not only give information about the mean number of particles produced, but also information about fluctuations and higher order moments of the probability distribution which are important tools for studying the underlying processes and mechanisms that operate. They are also useful in distinguishing various phenomenological models. Issues associated with fluctuations play an important role in many areas of physics and departures from Poisson statistics are of current interest. One purpose of this paper was an investigation of various models of particle multiplicity distributions that can be used in event-by-event analysis. These various phenomenological models are developed using a general form of a unified model which is based on a grand canonical partition function and an underlying weight arising from Feynman's path integral approach to statistical processes. A resulting distribution has three control parameters called a, x, z. The relationships of these parameters to various physical quantities are discussed. One important result is the connection of the parameter a to the Fisher exponent τ; namely $\tau = 2 - a$ for a generalized hypergeometric model called HGa. This connection arises from a parallel we developed between the model for particle multiplicity distributions considered here and our previous approach to cluster yields. Since an exact description of particle multiplicity distributions is not known, we have considered several cases with different τ's or a's which are contained in our unified description. Moreover, many of the existing distributions currently used in particle phenomenology are shown to be special choices of τ or a which appear in HGa. These include the Poisson distribution coming from coherent emission, chaotic emission producing a negative binomial distribution, combinations of coherent and chaotic processes leading to signal/noise distributions and field emission from Lorentzian line shapes producing the Lorentz/Catalan distribution called LC. Using the HGa model combinants, cumulants and moments are discussed and a physical significance is given to combinants in terms of the underlying partition weights of a Feynman path integral approach to statistical processes. The parameter a or Fisher exponent τ is shown to play an important role in the behavior of the combinants which manifest itself in various physical relationships. The HGa model and its associated special cases are used to explore a wide variety of phenomena. These include: linked pair approximations leading to hierarchical scaling relations on the reduced cumulant level, generalized void scaling relations, clan variable descriptions and their connections with stochastic variables and branching processes, KNO scaling behavior, enhanced non-Poissonian fluctuations. Models based on an underlying random walk description are also discussed.

In this paper we compared various particle multiplicity distributions within the hypergeometric model HGa. Our results show that even though various distributions have the same mean and fluctuation, the distribution itself or the underlying mechanism could be different. Comparisons within the HGa model also show that just comparing void variables χ and ξ or mean $\bar{n}$ and fluctuation f_2 or σ is not enough to distinguish different models that describe particle multiplicity data. Thus, to find the correct distribution and underlying mechanism from various data more information than just the mean and fluctuation are necessary and new variables should be found which are quite different between different models. For example, it is known [23,31] that higher order reduced factorial cumulants also need to be evaluated such as the third order cumulant κ_3.

Applications of our approach to the charged multiplicity data of L3 and H1 are given. The mean $\langle n\rangle$, fluctuation variable ξ, void scaling variable χ, and third order reduced cumulant variable κ_3 obtained from these experiments are compared with various models discussed in this paper. Both the HGa and GRW1D models, which have very similar multiplicity distributions as shown in Fig. 5, can fit the charged multiplicity data of L3. The HGa model can fit the H1 data up to its second order cumulant. However, it cannot give a negative third order cumulant. A small negative third order cumulant may be present in the H1 data reflecting an asymmetric distribution about a $\langle n\rangle$ with the $n < \langle n\rangle$ probability distribution spread out more than the $n > \langle n\rangle$ probability distribution. However, because of the very large error bars, positive values of κ_3 are not excluded and therefore no definite conclusions can be made about the applicability of an HGa model. The GRW1D model can accommodate a negative third order cumulant and more generally the oscillatory feature of the cumulants when a is taken as negative. This also requires a negative x and z. These properties associated with oscillatory features require further study.

In this paper we have also generalized the compound distribution that arises from sequential process which may reveal the dynamical structure of the distribution. Specifically, the underlying sequential picture involves a two-step process where the final distribution arises from the production of clusters followed by a subsequent decay of the clusters. For the HGa model, the final distribution is obtained from compounding a Poisson distribution of clusters with a NB distribution coming from the decay of each of the clusters. The HGa may arise through a three-step sequential process of Poisson–Poisson–Logarithmic compound distribution. It is also shown that the HGa can arise from a two-step sequential process of a NB distribution followed by a new HGa with a different mean value.

This work was supported in part by Grant No. 2001-1-11100-005-3 from the Basic Research Program of the Korea Science and Engineering Foundation and in part by the DOE Grant No. DE-FG02-96ER-40987.

Appendix A. Sequential procedures and compound Poisson distributions

In general, the underlying picture for a sequential process involves a two-step procedure in which the observed particles arise from the production of “clusters” with the subsequent decay of each cluster producing its distribution of particles. The final distribution is obtained by compounding the probability distribution of the clusters with another distribution coming from each cluster and summing over clusters. Specifically, the observed particles or members in system arise from production of $M = c$ clusters with probability distribution P_c. This is sequentially followed by each cluster decaying into k_α particles with the probability P_{k_α} with $\alpha = 1, 2, \ldots, c$. The probability of observing $n = \sum_k k n_k = \sum_\alpha k_\alpha$ particles is then obtained by a compound probability expression

$$P_n = \sum_c \sum_{\{k_\alpha\}} P_c \prod_{\alpha=1}^{c} P_{k_\alpha}. \tag{A.1}$$

Conclusions

- Mean charged multiplicity in AA collisions behaves like in e^+e^- collisions
- It is mainly determined by the energy going into collision
- More than two parameters are needed to describe the form of the multiplicity distribution (MD).
- Therefore in addition to the mean multiplicity and the width of the MD one should measure higher moments.